Title
Existence of the threshold pressure for seismic excitation by atmospheric disturbances

Permalink
https://escholarship.org/uc/item/263183kc

Journal
Geophysical Research Letters, 43(21)

ISSN
0094-8276

Authors
Tanimoto, Toshiro
Valovcin, Anne

Publication Date
2016-11-16

DOI
10.1002/2016gl070858

Peer reviewed

Existence of the Threshold Pressure in the Land-Atmosphere Interaction

Toshiro Tanimoto* and Anne Valovcin

Department of Earth Science and Earth Research Institute,

University of California, Santa Barbara, California 93106, USA.

*Corresponding author: Email toshiro@geol.ucsb.edu

Abstract

Excitation of seismic waves by atmospheric pressure changes is examined from data for two tropical cyclones, Tropical Storm Lee (2011) and Hurricane Isaac (2012). They moved through the Earthscope Transportable Array (USArray) and generated variations in pressure and ground motions that spanned 4-5 orders of magnitude in power spectral density (PSD). For vertical seismic ground velocity PSD (S_V) for frequencies between 0.01 and 0.02 Hz, there is a threshold pressure at about pressure PSD (S_P) of 10 (Pa^2s), below which vertical motion is not affected by local atmospheric pressure. Above this threshold pressure, vertical ground motion increases with surface pressure as $S_V \sim S_P^{1.5}$. In order to understand the land-atmosphere interaction, pressure above this threshold is the only useful range. Horizontal-component PSDs are about two orders of magnitude larger than vertical-component PSDs and change with pressure for its entire range. This overall trend is most likely caused by ground tilt.

Key Points:

- In the excitation of seismic waves by atmospheric pressure changes, there is a critical, threshold pressure.
- Below the threshold, vertical amplitudes are not affected by local atmospheric pressure changes.
- Horizontal amplitudes show the effects of tilt for the whole pressure range.

1. Introduction

How seismic signals are generated by the land-atmosphere interaction is an old question [e.g., Tanimoto et al., 2015]. It is a difficult question, mainly because of a lack of good, critical data sets. Good data in this case means a dense network of seismometers and barometers. We have noted that the Earthscope Transportable Array (TA hereafter) could provide unique data sets to address this question, although the principal purpose of TA was to improve our understanding of structure in the solid Earth. TA data became useful for the land-atmosphere interaction study after 2010, because high-quality barometers (SEED channel LDO) and infrasound sensors (SEED channel LDF) were added to this network (http://www.earthscope.org/science/observatories/usarray). We use the barometer data in this paper. Consistent results were obtained with the infrasound sensor data. Comparison between barometer and infrasound sensors is shown in Figure S1 (supplement) to support this point. Another pressure sensor, the MEMS pressure sensor (channel LDM), turned out to be inadequate for the frequency range (0.01-0.02 Hz) of this study.

In this paper, we focus on data for two tropical cyclones, Hurricane Isaac (2012) and Tropical Storm Lee (2011) that moved through the TA after their landfalls. Seismic and barometric data from these cyclones provide us unusual opportunities to observe the response of solid Earth generated by surface atmospheric pressure. Seismic ground motions and surface pressures varied 4-5 orders of magnitude in PSD as these hurricanes passed by.

We performed some analyses on Hurricane Isaac (Tanimoto and Lamontagne, 2014; Tanimoto and Valovcin, 2015) but in this paper we apply a different approach in order to understand some basic characteristics in the land-atmosphere interactions. In this paper, we only examine the co-located barometer and seismometer data and monitor how they change. The underlying idea is that the largest effects of atmospheric pressure should show up most clearly in the co-located seismic sensors. Despite the simplicity in this approach, we find quite interesting features in the relationships between surface pressure and ground motions. The most important point is the identification of the critical, threshold pressure; below this pressure, vertical ground motions are constant which means that seismic amplitudes are independent of changes in local atmospheric pressure. Above this pressure, ground motions increase with pressure. It shows that there exists a threshold atmospheric pressure, above which atmospheric pressure overwhelms other sources of seismic noise.

We will describe the data and our approach in section 2, three main characteristics in data in section 3 and our interpretations in section 4.

2. Data and Our Approach

Figure 1 shows the tracks of Hurricane Isaac and Tropical Storm Lee in the top panels. Red circles in top panels show the locations of stations (TA and some permanent stations) that had both seismometer and barometer data. Blue circles are stations with seismometers only. Since barometers were installed starting in mid-2010, only the eastern half had barometers at the time of Lee (Figure 1, top-right).

Although the tracks of both tropical cyclones are near the edge of the TA, we could confirm that seismic amplitudes and pressure variations are consistent with (approximate) cylindrical symmetry, at least for available azimuths, and they decreased with distance from the centers. The bottom panels show examples for selected time intervals; we chose UTC 08:00, August 29, 2012 for Isaac (Figure 1 bottom, left) and UTC 10:00, September 3, 2011 for Lee (Figure 1 bottom, right). Each circle is an average PSD for frequencies between 0.01 and 0.02 Hz. Seismic velocity PSDs are shown in blue with scale on the left and pressure PSDs are shown in red with scale on the right.

We mainly focus on this low frequency range (0.01-0.02 Hz) because seismic and pressure amplitudes decay systematically with distance from the cyclone centers. Strictly speaking, the amplitudes peak at about 50-100 km from the centers, presumably at the location of the eyewall [Tanimoto and Lamontagne, 2014], and decay outward. Most stations turn out to be outside this (eyewall) peak.

Figure 1 shows only vertical-component seismic data (bottom panels). For comparison, we show Figure S2 (supplement) that shows amplitude-distance variations of three component seismic data (0.01-0.02 Hz) at UTC 12:00, August 29, 2012, for Isaac. Similar amplitude decay trends are seen for all components but horizontal data contain much larger scatter.

We checked higher frequency signals up to the microseism frequency bands (0.05-0.5 Hz) [Tanimoto and Valovcin, 2015] but these decaying trends with distance were lost in high frequency signals. It appears that higher frequency waves are mostly generated by ocean waves that are excited by hurricane winds, and thus the source area for these high-frequency waves seems quite broad. On the other hand, the amplitudes in our chosen frequency band (0.01-0.02 Hz) show that they decay with distance from the center and support the view that they were generated close to the center of the hurricanes.

Two bottom panels in Figure 1 show that the influence zone of hurricanes is mostly within 1000 km from their centers, with particularly large effects confined to the innermost 500 km. Some deviations to this statement can be recognized outside 1000 km as there is a secondary peak of pressure about 1500 km [Figure 1, bottom panels]. Associated seismic amplitudes to these pressure variations are quite small and remain within the scatter of short-distance (<1000 km) data [Figure S3, supplement]. We believe these secondary peaks around 1500 km were caused by spiral winds and rain bands that extend outward from the central region. But since they do not bring much information on the land-atmosphere interaction, as evidenced in Figure S3, we focus our analysis on data within 1000 km from the cyclone centers.

3. Pressure PSD vs. Ground Velocity PSD

Figure 2 shows plots of surface pressure PSD (horizontal axis) vs. ground velocity PSD (vertical axis). Three-component ground velocity PSDs are indicated by three colors, vertical (Z) in blue, radial (R) in red and transverse (T) in black. Radial and transverse components were obtained by using the locations of the center of Isaac and Lee, reported in Brown [2011] for Lee and Berg [2013] for Isaac respectively.

Each point in Figure 2 represents PSDs computed for a time-series length of 1 hour. The entire time interval of data that was used to create Figure 2 was three days (August 29-31, 2012 for Isaac and September 3-5, 2011 for Lee).

Vertical-component data (blue) and horizontal-component data (red and black) make two separate clusters in Figure 2 when plotted against surface pressure from the co-located barometers. Horizontal-component PSDs are typically larger than vertical-component PSDs by about 2-3 orders of magnitude. Green dash lines in Figure 2 were determined by the least squares, fitting the formula $\log_{10}(S_V)=A \log_{10}(S_P)+B$ for different pressure ranges. In this formula, S_V is the ground velocity PSD and S_P is the surface pressure PSD. The coefficients determined by this fitting process (A and B) are summarized in Table 1. In total, there are five independent lines in Figures 2 and 3 and each line is denoted by its name (V_g, V_{L1}, V_{L2}, H_g and H_L).

Both vertical and horizontal data were fit separately below and above the threshold pressure (PSD) S_P=10 (Pa^2s). This threshold pressure was first chosen from vertical-component data that show clear a break in the data. We overlay the vertical PSDs from two cyclones in Figure 3 (top). Because Isaac was much stronger than Lee, we can see more points in higher pressure ranges for Isaac but the threshold pressure seems to agree between the two cyclones.

By fitting data from both cyclones above S_P=10, the dash line denoted by V_g was obtained. For the vertical-component data below this threshold value, we obtained V_{L2}. The latter is constant as the coefficient A was set to zero. There is a slight difference on this constant value between Isaac and Lee. In order to indicate this difference, we denote the value for Isaac by V_{L1} (Table 1) but it is not significantly different from V_{L2} that was determined from the combined vertical-component data. But this difference indicates that the background noise level, created by other noise sources, varies seasonally and sometimes year to year. If we took into account the differences between these flat noise levels from two cyclones, the threshold value (S_P=10) can vary from S_P=5 to 20 approximately.

Existence of a threshold value is not so obvious in horizontal-component data in Figure 2. It is partly because an overall trend in horizontal data shows a large gradient for the entire pressure range (Figures 2 and 3). We believe this overall trend in gradient is caused by the well-known ground tilt. Tilt causes the same effect with horizontal acceleration and is particularly large in low-frequency bands below 0.02 Hz [e.g., Aki and Richards, 2002; Farrell, 1969; Rodgers, 1968].

There is an additional feature in horizontal data; if we overlay data from two tropical cyclones (Figure 3, bottom), there is a hint that the gradient becomes steeper as pressure increases. The least squares fits below and above S_P=10 (lines H_g and H_L) clearly show a steepening trend in gradient. Although we used two lines to fit horizontal data in Figure 3, in terms of underlying physical processes, it is hard to imagine a threshold pressure for horizontal data that causes a sudden change. We interpret that this gradient increase occurs gradually.

But why does the gradient in horizontal data increase with pressure? We speculate that there exists a direct wind effect for high pressure ranges. In general, pressure fluctuation for a frequency range 0.01-0.02 Hz is controlled by winds and is nearly proportional to the square of wind velocity. Therefore, some effects of wind are already included in pressure changes. But when the wind becomes strong, it can exert forces directly on nearby trees and observational facilities and generate additional ground tilt. This should be in addition to surface pressure changes and thus could be a cause for an increase in gradients in Figure 3. However, this is a speculation and details are hard to verify with current data sets.

In Figure 4, we show similar seismic amplitudes vs. pressure plot for Tropical Storm Lee for four different frequencies, 0.01-0.02 Hz (top left), 0.04-0.05 Hz (top right), 0.09-0.10 Hz (bottom left) and 0.14-0.15 Hz (bottom, right). Amplitude differences between horizontal-component data and vertical-component data are the largest for 0.01-0.02 Hz and quite large for 0.04-0.05 Hz. Both panels at top show that horizontal amplitudes increase with pressure amplitudes (PSD). The differences in vertical and horizontal amplitudes decrease in higher frequency plots and the correlation between horizontal amplitudes and pressure amplitudes also becomes smaller. In the panel for 0.09-0.10 Hz, there may still be a weak correlation for pressure above 1-10 (Pa^2s) but in the 0.14-0.15 Hz plot, seismic amplitudes change little with local surface pressure. Clearly the dominance of local atmospheric effects is confined to low frequencies below about 0.05 Hz. It should also be noted that these higher-frequency signals in the bottom panels are mostly the secondary microseism (seismic noise) that are generated in the oceans [Longuet-Higgins, 1950; Hasselman, 1963].

4. Discussion and Summary

One of the most robust features in our observation is the existence of a threshold pressure in vertical-component data at a pressure PSD of about $S_P=10$ (Pa^2s). Because of scatter in data, this value contains some uncertainties and can vary from $S_P=5$ to 20. Below this threshold pressure, vertical amplitudes do not change with pressure. This lack of correlation means that the local atmospheric pressure is not the main source of seismic ground motion (noise) at the site. These signals below the threshold pressure were generated by processes other than the local atmospheric pressure, such as ocean waves away from the station. The threshold pressure can be viewed as the pressure when the effects of the local atmospheric pressure exceed those of other seismic-noise sources. In order to understand the land-atmosphere interaction in more details, we must focus on the pressure range above this threshold.

We take a view that atmospheric pressure acts as an excitation source at Earth's surface for seismic waves. In the whole, coupled Earth system, this view may not apply if phase velocity of atmospheric waves were close to phase velocity of seismic waves in the solid Earth as the transmission of waves become very efficient between the atmosphere and the solid Earth. But such a match in phase velocity is not likely to occur as atmospheric waves have velocities of a few hundred meters per second and seismic waves have velocities of 3-4 km/s for surface waves and faster body waves. It was pointed out previously [Sorrells, 1971; Sorrells and Goforth, 1973] that atmospheric pressure acts almost as a surface load under such a condition. Seismic data show such amplitude behaviors to first order, although they should also contain some smaller-amplitude propagating surface waves. But those seismic data are in the near-field and seem to be dominated by pressure loading effects.

The proportionality constant (A in the log-log formula) between S_V and S_P in Figure 2 (and 3) is not 1 above the threshold pressure. Instead, it is about 1.5 (V_g in Table 1). We interpret this observation as follows; the excitation of seismic ground motion by atmospheric pressure occurs by a force that can be considered to be a random force. This is because atmospheric pressure has very short correlation distance on Earth's surface (about 100 m or less). It changes its sign with short wavelengths of the order of 10-100 m [e.g., Herron et al., 1969; McDonald et al, 1971]. On the other hand, the pressure source is spread out over many kilometers. In essence, we have a rapidly fluctuating source that extends over a large area. In such a case, one can approximate that the excited seismic ground motion PSDs become proportional to pressure PSD by $S_V \propto L^2 S_P$ where L is the correlation length in the surface pressure field [e.g., Kobayashi and Nishida, 1998; Fukao et al., 2002; Tanimoto, 2005; Tanimoto and Valovcin, 2015]. In such a model, if the correlation length L is proportional to $S_P^{0.25}$, the gradient of 1.5 can be explained. This means that the correlation length changes with pressure. Physically, one would expect that larger pressure is related to stronger wind. If strong lateral wind exists, one can imagine that the correlation length in the surface pressure field should become larger as pressure at a location can be transported to nearby location by winds. However, why the exponent becomes 0.25 is left unexplained. Understanding it requires a careful theoretical study.

Acknowledgments

All data were obtained from the data center at IRIS (Incorporated Research Institutions for Seismology). We appreciate accessibility of these data and their efficient service. This study was partially supported by NSF-EAR 1547523.

References

Aki, K. and P. Richards (2002), *Quantitative Seismology*, second edition, University Science Books, Sausalito, California.

Berg, R. (2013), Tropical Cyclone Report: Hurricane Isaac (AL092012) 21 August – 1 September 2013, NOAA/National Weather Service, Miami, FL.

Brown, D. P. (2011), Tropical Cyclone Report: Tropical Storm Lee (AL132011), 2-5 September, 2011, National Hurricane Center.

Farrell, W. (1969). A gyroscopic seismometer: measurement during the Borrego earthquake, Bull. Seism. Soc. Am., 59, 1239-1246.

Fukao Y, Nishida K, Suda N, Nawa K, Kobayashi N., 2002. A theory of the Earth's background free oscillations, *J. Geophys. Res.,* 107, B9, 2206, doi:10.1029.

Hasselmann, K. A. (1963). A statistical analysis of the generation of microseisms, *Rev. Geophys.*, 1, 177-209.

Herron, T. J., I. Tolstoy, and D. W. Kraft (1969). Atmospheric pressure background fluctuations in the mesoscale range, *J. Geophys. Res.,* 74, 1321-1329.

Kobayashi, N. and K. Nishida (1998). Continuous excitation of planetary free oscillations by atmospheric disturbances, Nature, 395, 357-360.

Longuet-Higgins, M. S. (1950). A theory of the origin of microseisms, *Philos. Trans. R. Soc. London, Ser. A*, 243, 1-35.

McDonald, J. A., E. J. Douze, and E. Herrin (1971). The structure of atmospheric turbulence and its application to the design of pipe arrays, *Geophys. J. R. Astr. Soc.*, 26, 99-106.

Rodgers, P. (1968). The response of the horizontal pendulum seismometer to Rayleigh and Love waves, tilt and free oscillations of the Earth, Bull. Seism. Soc. Am., 58, 1384-1406.

Sorrells, G. (1971). A Preliminary Investigation into the Relationship between Long-Period Seismic Noise and Local Fluctuations in the atmospheric Pressure Field, Geophys. J. R. astr. Soc., 26, 71-82.

Sorrells, G. and T. Goforth (1973). Low-frequency Earth motion generated by slowly propagating partially organized pressure fields, Bull. Seism. Soc. Am., 63, 1583-1601.

Tanimoto, T. (2005). The Oceanic Excitation Hypothesis for the Continuous Oscillations of the Earth, *Geophys. J. Int.,* 160, 276-288.

Tanimoto, T., K. Heki, and J. Artru-Lambin (2015). Interaction of Solid Earth, Oceans, Atmosphere and Ionosphere, In: Gerald Schubert (editor-in-chief) Treatise on Geophysics, 2nd edition, Oxford: Elsevier; 2015. pp. 421-443.

Tanimoto, T. and A. Lamontagne (2014). Temporal and spatial evolution of an on-land hurricane observed by seismic data, Geophys. Res. Lett., 41, 7532–7538, 2014, doi:10.1002/2014GL061934

Tanimoto, T., and A. Valovcin (2015), Stochastic excitation of seismic waves by a hurricane, J. Geophys. Res. Solid Earth, 120, 7713–7728, doi:10.1002/2015JB012177.

Table 1: Least squares fit by the formula $\log_{10}(Sv)=A \log_{10}(Sp)+B$ for various ranges. IDs are the same in Figures 2, 3 and 4. Ranges of barometer (pressure) PSD are in the second column. V_{L1} is for Isaac only but all others were derived for the combined data of Isaac and Lee.

ID	Range (S_P)	A	B
V_g	$S_P > 10$	1.501 ± 0.001	-17.20 ± 0.08
V_{L1}	$S_P < 10$	0.0	-15.70 ± 0.02
V_{L2}	$S_P < 10$	0.0	-15.52 ± 0.02
H_g	$S_P > 10$	1.261 ± 0.020	-13.71 ± 0.02
H_L	$S_P < 10$	0.618 ± 0.031	-13.26 ± 0.03

Figure Captions

Figure 1: (top, left) Track of Hurricane Isaac (August, 2012) and seismic stations from Earthscope. Black circles are the locations of its center at every six hours. Green circles indicate the midnight of each day. Red circles indicate stations had barometer and seismometer. Blue circles indicate stations with seismometer only. (top, right) Track of Tropical cyclone Lee (September, 2011). (bottom, left) Seismic vertical PSD and pressure PSD plotted against distance from the center of Isaac. (bottom, right) Seismic vertical PSDs and pressure PSDs for Lee.

Figure 2: Seismic amplitudes (PSD) plotted against pressure PSD for every 1-hour interval. Top is for Hurricane Isaac and bottom is for Tropical Storm Lee. Vertical PSDs are denoted by blue circles, radial by red and transverse by black. Lines by the least-squares fit are shown by green dashes. Except for V_{L1}, they were derived from the combined data set for Isaac and Lee. Hg is for horizontal component data above the threshold value S_P=10. H_L is for horizontal component data below this threshold pressure. V_g is for vertical component data above the threshold pressure, determined from the combined data from both tropical cyclones. V_{L1} is for below the threshold for Isaac only. V_{L2} is for the combined data of Isaac and Lee. The coefficients are in Table 1.

Figure 3: Same data as in Figure 2 but the data from Isaac and Lee were overlaid. Top is the vertical component data and bottom is the horizontal component data. Lines are the same with those in Figure 2.

Figure 4: Seismic amplitudes (PSD) vs. pressure PSD for four frequency ranges, 0.01-0.02 Hz (top, left), 0.04-0.05 Hz (top, right), 0.09-0.10 Hz (bottom, left) and 0.14-0.15 Hz (bottom, right). Because of tilt, horizontal component data have much larger

amplitudes than vertical component data for lower frequency ranges (0.01-0.02 and 0.04-0.05 Hz) and have good correlation with local pressure data. In higher frequency ranges (0.09-0.10 and 0.14-0.15 Hz), tilt effects are much smaller and vertical and horizontal components have similar amplitudes. In the 0.14-0.15 Hz plot, signals are generated in the ocean and do not show much correlation with local atmospheric pressure.

Figure 1.

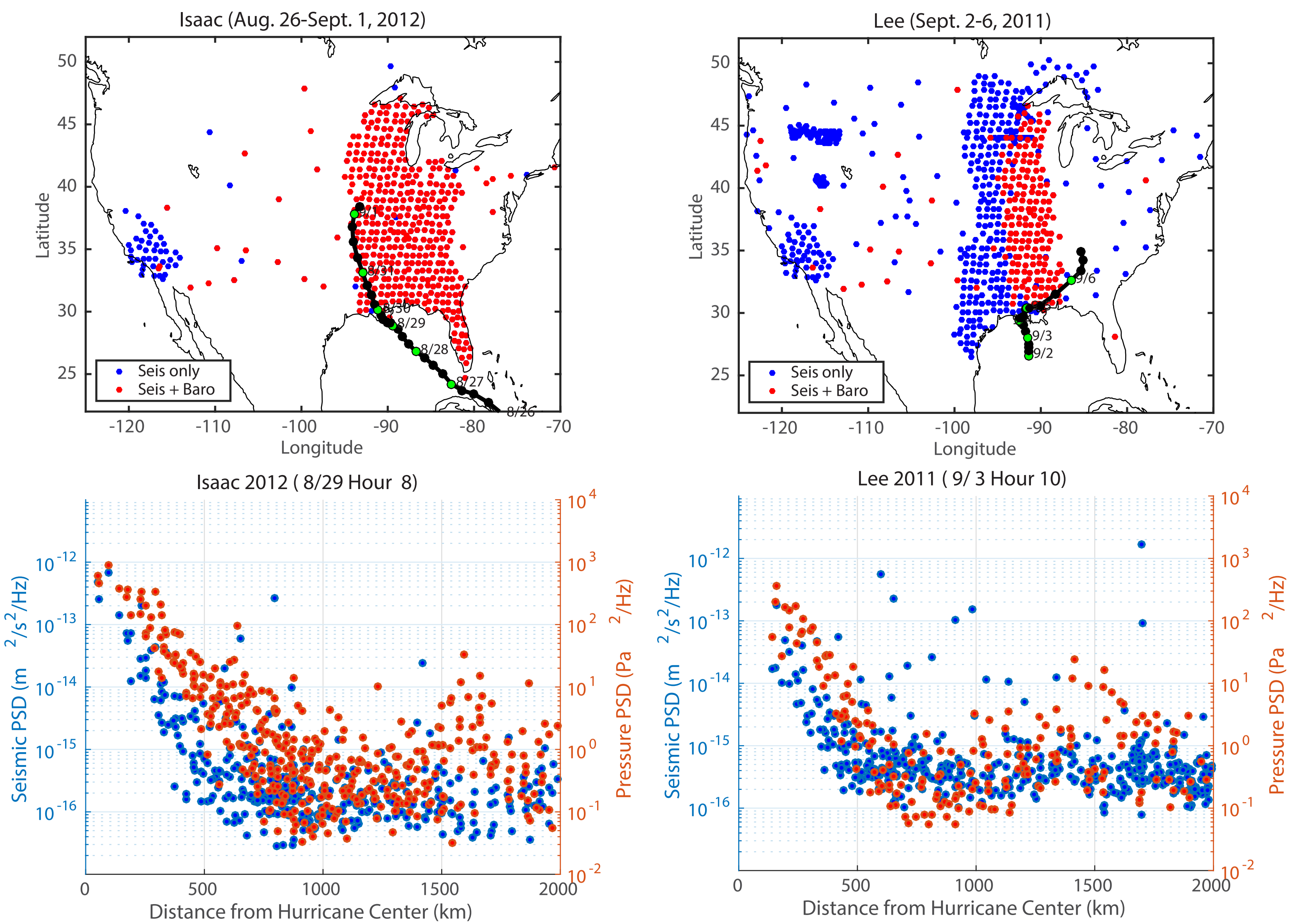

Isaac (Aug. 26-Sept. 1, 2012)
Latitude
Longitude
Seis only
Seis + Baro
8/26
8/27
8/28
8/29
8/30
Lee (Sept. 2-6, 2011)
9/2
9/3
9/6
Isaac 2012 (8/29 Hour 8)
Lee 2011 (9/ 3 Hour 10)
Seismic PSD (m²/s²/Hz)
Pressure PSD (Pa²/Hz)
Distance from Hurricane Center (km)

Figure 2.

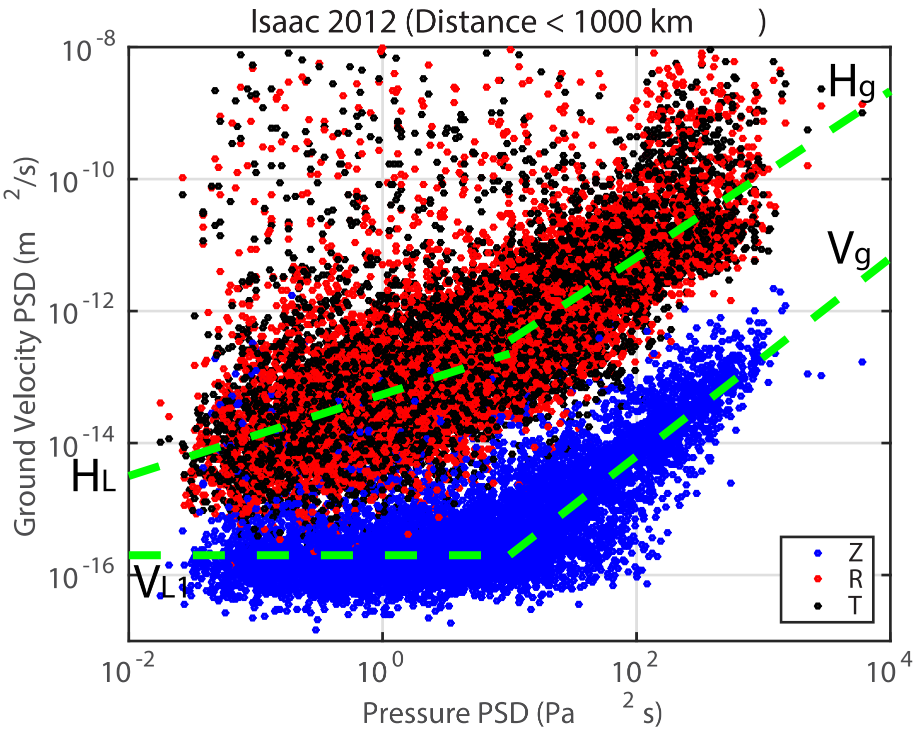

Isaac 2012 (Distance < 1000 km)
Ground Velocity PSD (m 2/s)
Pressure PSD (Pa 2 s)
Hg
Vg
HL
VL1
Z
R
T

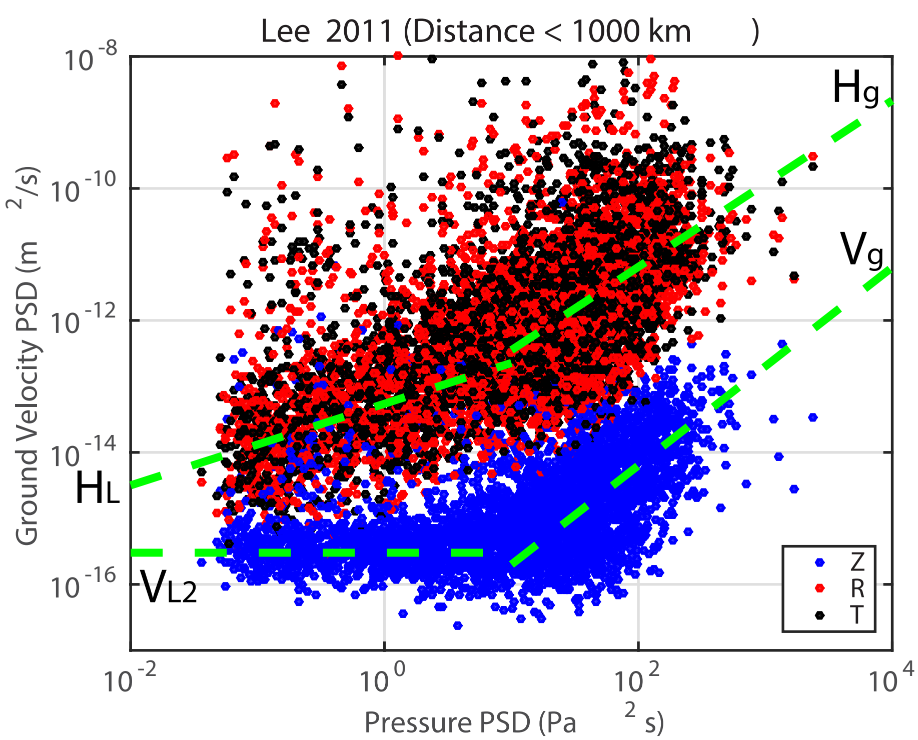

Lee 2011 (Distance < 1000 km)
Ground Velocity PSD (m 2/s)
Pressure PSD (Pa 2 s)
Hg
Vg
HL
VL2
Z
R
T

Figure 3.

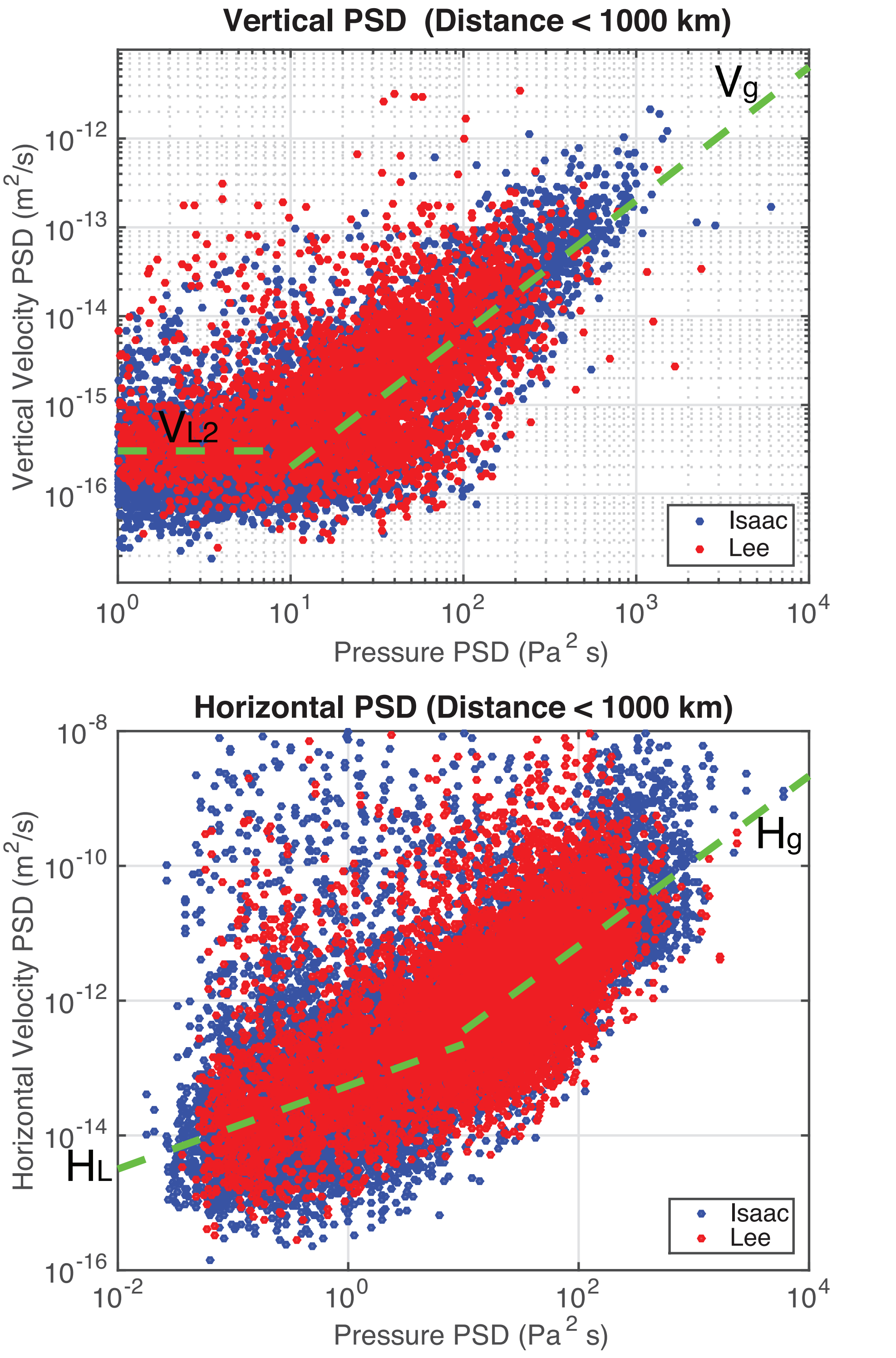

Vertical PSD (Distance < 1000 km)
Vertical Velocity PSD (m^2/s)
Pressure PSD (Pa^2 s)
V_g
V_L2
Isaac
Lee
Horizontal PSD (Distance < 1000 km)
Horizontal Velocity PSD (m^2/s)
Pressure PSD (Pa^2 s)
H_g
H_L
Isaac
Lee

Figure 4.

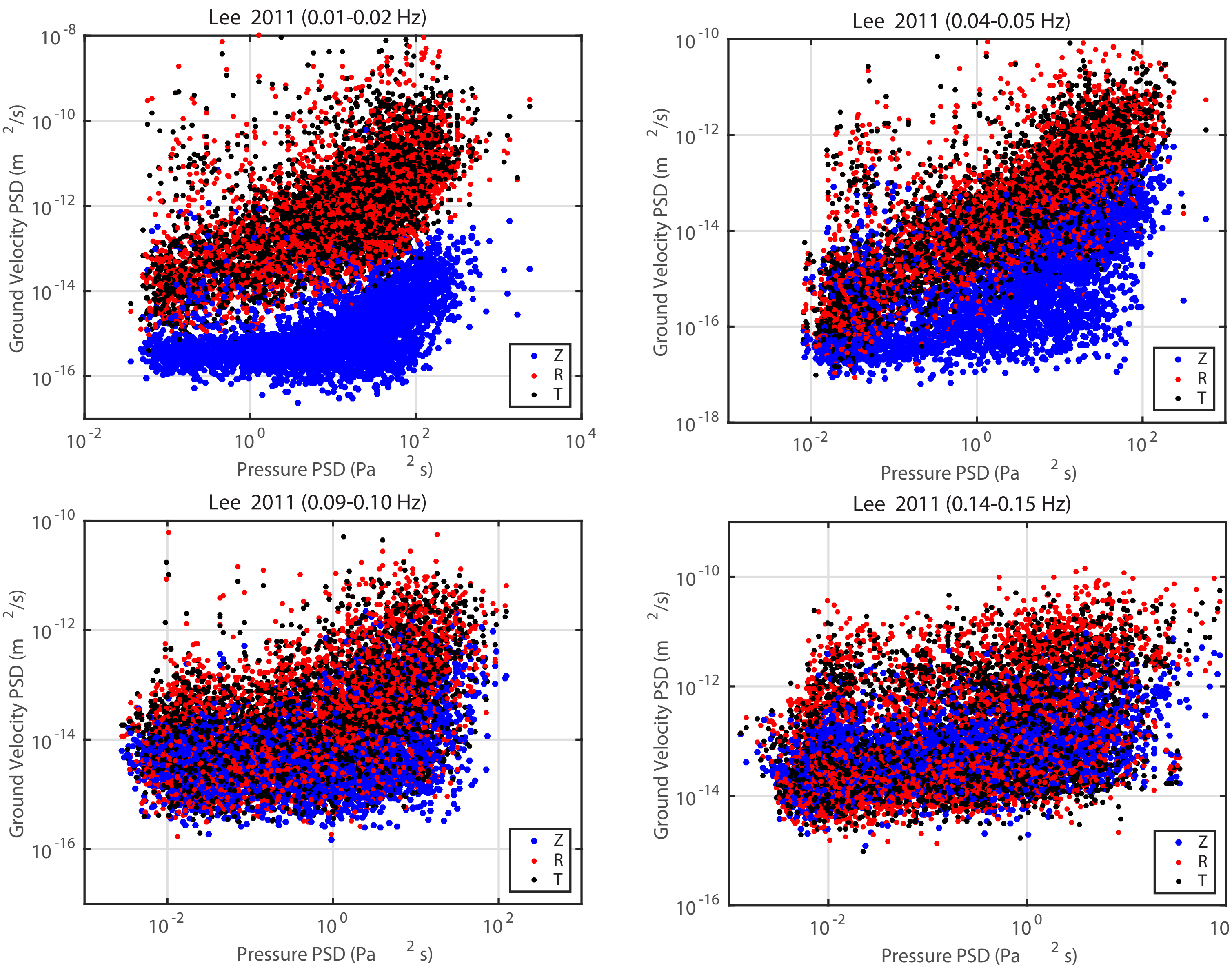

Lee 2011 (0.01-0.02 Hz)
Ground Velocity PSD (m 2/s)
Pressure PSD (Pa 2 s)
Z
R
T
Lee 2011 (0.04-0.05 Hz)
Ground Velocity PSD (m 2/s)
Pressure PSD (Pa 2 s)
Z
R
T
Lee 2011 (0.09-0.10 Hz)
Ground Velocity PSD (m 2/s)
Pressure PSD (Pa 2 s)
Z
R
T
Lee 2011 (0.14-0.15 Hz)
Ground Velocity PSD (m 2/s)
Pressure PSD (Pa 2 s)
Z
R
T